Design, Implementation and Experiments of a Robust Passivity-based Controller for a Rolling-balancing System

Martin Crespo[1], Alejandro Donaire[2,3], Fabio Ruggiero[2], Vincenzo Lippiello[2] and Bruno Siciliano[2]
[1]*Departamento de Control, FCEIA, Universidad Nacional de Rosario and CONICET, Riobamba 245 bis, S2000EKE, Rosario, Argentina*
[2]*PRISMA Lab, Dipartimento di Ingegneria Elettrica e Tecnologie dell'Informazione, Università degli Studi di Napoli Federico II, Via Claudio 21, 80125, Napoli, Italy*
[3]*School of Engineering, The University of Newcastle, University Drive, 2308, NSW, Newcastle, Australia*

Keywords: Rolling-ballancing System, Nonlinear Control, Lyapunov Methods, Passivity.

Abstract: In this paper, we present the design of a robust interconnection and damping assignment controller for a rolling-balancing system known as the disk-on-disk. The underactuation feature of this system hampers the control design, and since we consider matched disturbances, the problem becomes even more challenging. To overcome this difficulty, we propose to design first a controller to stabilize the desired equilibrium of the case where the disturbance is not present, and then we robustify this controller by adding a nonlinear PID outer loop that compensates the disturbance. Finally, we evaluate the practical applicability of the control design by implementing the controllers on a real hardware for the disk-on-disk system.

1 INTRODUCTION

Control theory has provided a rich variety of methods for control design of nonlinear systems (Khalil, 2002; Haddad and Chellaboina, 2007). In the context of robotics and mechanical systems, nonlinear methods have been widely used for control design (see e.g. (Siciliano et al., 2009; Spong et al., 2006)). A class of mechanical systems posing a particularly challenging control problem is that of underactuated mechanical systems. Underactuation refers to the fact that number of the inputs is smaller than the number of the degrees of freedom.

Passivity-based control (PBC) has shown to be a successful technique for control design of underactuated systems (Ortega et al., 1998). A classical constructive method for stabilization of mechanical system is the so-called interconnection and damping assignment (IDA) (Ortega et al., 2002). This technique is based on Lagrange-Dirichlet result on stability of mechanical systems, which states that an isolated minimum of the potential energy is Lyapunov stable (see (Merkin, 1997, Theorem 3.1) for details). The basic idea of IDA-PBC is to shape the energy of the system and assign a minimum at the desired equilibrium by using feedback measurements and the control input. A further injection of damping is needed to ensure asymptotic stability (Ortega et al., 2016). To stabilize a desired equilibrium for fully actuated systems, only the potential energy of the system is needed to be shaped. However, both the potential and kinetic energies have to be shaped to stabilize underactuated systems, a procedure known as total energy shaping. Although passivity-based controllers are known to be robust against parameter uncertainties, the action of external disturbances can deteriorate the performance of the closed loop or, even worse, produce instabilities. To address this problem, a classical addition of control actions has been proposed in (Donaire and Junco, 2009; Ortega and Romero, 2012). This integral action design has been specialised for fully actuated and underactuated mechanical system by (Romero et al., 2013) and (Donaire et al., 2016), respectively.

In this paper, we consider the control problem of the disk-on-disk (DoD), which is an underactuted rolling-balancing system (Ryu et al., 2013). The DoD is a case study of *nonprehensile manipulation* and has been used as testbed for control designs in this context (Lippiello et al., 2016). In addition to the standard stabilization problem, we also consider input disturbances, which complicate the design. Previous works have considered the stabilization problem of the DoD using exact-feedback linearization (Ryu

Crespo, M., Donaire, A., Ruggiero, F., Lippiello, V. and Siciliano, B.
Design, Implementation and Experiments of a Robust Passivity-based Controller for a Rolling-balancing System.
DOI: 10.5220/0005981700790089
In *Proceedings of the 13th International Conference on Informatics in Control, Automation and Robotics (ICINCO 2016) - Volume 2*, pages 79-89
ISBN: 978-989-758-198-4

et al., 2013) and backstepping (Ryu et al., 2012), but none of these works consider disturbances in the design. In our work, we explicitly consider the disturbances and we design a robust IDA-PBC controller following the approach proposed by (Donaire et al., 2016). This controller results in a classical IDA-PBC inner controller plus a nonlinear PID-type outer-loop controller, which rejects the disturbance. In addition, we implement the control laws in a real hardware for the disk-on-disk prototype, and run a set of experiments. These experiments allow assesing the performance of the controllers and evaluating the practical applicability of the methods provided in the literature of control theory.

The rest of the paper is organized as follows: Section 2 reviews the basic background on port-Hamiltonian framework and IDA-PBC. The control design for the disk-on-disk is developed in Section 3. Section 4 presents the experiment results. Finally, the paper is wrapped-up with the conclusions.

Notation. The matrix I_n is the $n \times n$ identity matrix. Given a function $H : \mathbb{R}^n \to \mathbb{R}$ we define $\nabla_x H \triangleq \left(\frac{\partial H}{\partial x}\right)^T$. To simplify the notation, we drop the dependency of functions and matrices of their independent variables when this dependency is clear from the context.

2 PORT-HAMILTONIAN SYSTEMS

2.1 Hamiltonian Models

A large class of mechanical systems can be described by Euler-Lagrange equations of motion

$$\frac{d}{dt}\left[\nabla_{\dot{q}}\mathcal{L}(q,\dot{q})\right] - \nabla_q \mathcal{L}(q,\dot{q}) = G(q)u, \qquad (1)$$

where $q \in \mathbb{R}^n$ is the generalized position, u the input force, $G : \mathbb{R}^n \to \mathbb{R}^{n\times m}$ is the input matrix and $\mathcal{L}$ the Lagrangian

$$\mathcal{L}(q,\dot{q}) = \frac{1}{2}\dot{q}^\top M(q)\dot{q} - V(q),$$

where $V : \mathbb{R}^n \to \mathbb{R}$ is the potential energy and $M : \mathbb{R}^n \to \mathbb{R}^{n\times n}$ is the mass matrix and satisfies the condition $M(q) = M^T(q) > 0$. Applying the Legendre transformation and defining the generalized momentum $p = M(q)\dot{q}$ (Lanczos, 1960), we can express the dynamics (1) in the Hamiltonian form as follows

$$\begin{bmatrix}\dot{q}\\ \dot{p}\end{bmatrix} = \begin{bmatrix}0_{n\times n} & I_n\\ -I_n & 0_{n\times n}\end{bmatrix}\begin{bmatrix}\nabla_q H\\ \nabla_p H\end{bmatrix} + \begin{bmatrix}0_{n\times m}\\ G(q)\end{bmatrix}u \qquad (2)$$

where $p \in \mathbb{R}^n$ and $H : \mathbb{R}^{n\times n} \to \mathbb{R}$ is the total energy system given as

$$H(q,p) = \frac{1}{2}p^\top M^{-1}(q)p + V(q). \qquad (3)$$

2.2 Energy Shaping and Damping Assignment

The stabilization problem of the system (2) using IDA-PBC is to find a control input u such that the dynamics of the closed loop can be written as a port-Hamiltonian system as follows

$$\begin{bmatrix}\dot{q}\\ \dot{p}\end{bmatrix} = \begin{bmatrix}0_{n\times n} & M^{-1}M_d\\ -M_d M^{-1} & J_2 - R_d^\top\end{bmatrix}\begin{bmatrix}\nabla_q H_d\\ \nabla_p H_d\end{bmatrix} \qquad (4)$$

where the matrices $J_2(q,p) = J_2^\top(q,p)$ and $R_d(q) = G^\top(q)K_v G(q)$ represent the desired interconnection and damping structures, respectively, and $K_v > 0$ is a free symmetric matrix to be chosen. The function $H_d : \mathbb{R}^n \to \mathbb{R}$ is the desired energy in closed loop which has the form

$$H_d(q,p) = \frac{1}{2}p^\top M_d^{-1}(q)p + V_d(q) \qquad (5)$$

where $M_d(q) = M_d^\top(q) > 0$ and $V_d(q)$ are the desired mass matrix and the desired potential energy of the closed loop, respectively. In addition, if $q^\star$ is a minimum of the potential energy, then the desired energy H_d qualifies as a Lyapunov candidate function, and its time derivative along the solutions of (4) results as follows

$$\dot{H}_d = -p^\top M_d^{-1} G^\top K_v G M_d^{-1} p \leq 0, \qquad (6)$$

which ensures that $q^\star$ is a stable equilibrium of the closed-loop system. Moreover, asymptotic stability follows if the signal $y_d = GM_d^{-1}p$ is detectable (Ortega et al., 2002).

The classical approach to design an IDA-PBC controller is to compute the control in two steps. First, the energy shaping control $u_{\mathtt{ES}}$, and second the damping injection $u_{\mathtt{DI}}$. Then, the control input is obtained as $u = u_{\mathtt{ES}} + u_{\mathtt{DI}}$. The energy shaping controller is computed by matching the open dynamics (2) and the desired closed loop (4) assuming $R_d = 0$. This procedure results in the following matching equation

$$\begin{bmatrix}0_{n\times n} & I_n\\ -I_n & 0_{n\times n}\end{bmatrix}\begin{bmatrix}\nabla_q H\\ \nabla_p H\end{bmatrix} + \begin{bmatrix}0_{n\times m}\\ G(q)\end{bmatrix}u_{\mathtt{es}} = \begin{bmatrix}0_{n\times n} & M^{-1}M_d\\ -M_d M^{-1} & J_2\end{bmatrix}\begin{bmatrix}\nabla_q H_d\\ \nabla_p H_d\end{bmatrix}, \qquad (7)$$

which should be solve for $u_{\mathtt{ES}}$. For the nontrivial case of underactuated systems, where $G(q)$ is full column rank but non invertible matrix, the solution of (7) can be found by solving the following two equations:

- Kinetic-energy matching equation (KE-ME)

$$G^{\perp}\Big\{\nabla_q\left[p^T M^{-1} p\right] - M_d M^{-1}\times \nabla_q\left[p^T M_d^{-1} p\right] + 2J_2 M_d^{-1} p\Big\} = 0 \tag{8}$$

- Potential-energy matching equation (PE-ME)

$$G^{\perp}\Big\{\nabla_q V - M_d M^{-1}\nabla_q V_d\Big\} = 0, \tag{9}$$

where $G^{\perp} \in \mathbb{R}^{(n-m)\times n}$ is the full rank left annihilator of G, i.e. $G^{\perp}G = 0$. Then, the energy shaping control law is given by

$$u_{\mathtt{ES}} = (G^{\top}G)^{-1}G^{\top}\Big[\nabla_q H - M_d M^{-1}\nabla_q H_d + J_2\nabla_p H_d\Big]. \tag{10}$$

The second step in the design is the damping injection, which is given by the control law

$$u_{\mathtt{DI}} = -K_v G^{\top} M_d^{-1} p. \tag{11}$$

As discussed by (Ortega et al., 2002), the injection of damping together with the detectability condition are needed for asymptotic stability.

3 CONTROL DESIGN FOR THE DISK-ON-DISK

3.1 Dynamic Model

The DoD is a rolling-balancing system shown in Figure 1. Disk 1 is actuated by a controlled torque whilst Disk 2 is non-actuated (see (Ryu et al., 2013) for a detailed modelling development). The control objective is to stabilise Disk 2 at the upright position while driving the angle of Disk 1 to a target reference.

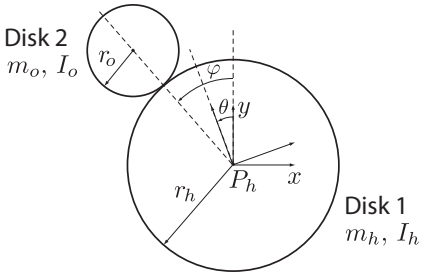

Figure 1: A schematic of the DoD system.

The dynamic model of the DoD can be described by the Lagrangian equations in coordinates (θ, φ), where θ is the angle of Disk 1, and φ is the deviation angle of Disk 2 respect to the upright position. The Langrangian for the DoD is given by

$$\mathcal{L}(q,\dot{q}) = \frac{1}{2}\begin{bmatrix}\dot{\theta} & \dot{\varphi}\end{bmatrix}^T \begin{bmatrix}M_{11} & M_{12}\\ M_{21} & M_{22}\end{bmatrix}\begin{bmatrix}\dot{\theta} & \dot{\varphi}\end{bmatrix} - V(q) \tag{12}$$

where

$$V(q) = V_0\cos(\varphi)$$

with $V_0 = m_o g(r_o + r_h)$. The function V represents the potential energy and M is the mass matrix whose entries are

$$M_{11} = r_h^2(m_o + m_h)$$
$$M_{12} = M_{21} = -m_o r_h(r_o + r_h)$$
$$M_{22} = 2m_o(r_o + r_h)^2$$

Equivalently, as explained in Section 2, the DoD model can be written in the Hamiltonian form as follows

$$\begin{bmatrix}\dot{q}\\ \dot{p}\end{bmatrix} = \begin{bmatrix}0 & I\\ -I & 0\end{bmatrix}\begin{bmatrix}\nabla_q H\\ \nabla_p H\end{bmatrix} + \begin{bmatrix}0\\ G\end{bmatrix} u \tag{13}$$

where the coordinates $q = \begin{bmatrix}\theta & \varphi\end{bmatrix}^{\top}$, the momenta $p = M\dot{q}$ and the input matrix $G = \begin{bmatrix}1 & 0\end{bmatrix}^{\top}$. The Hamiltonian function is

$$H(q,p) = \frac{1}{2}p^T M^{-1} p + V(q).$$

3.2 Energy Shaping and Damping Assignment Control

The objective is to design a IDA-PBC controller for the DoD system that stabilises the point $q^* = (\theta^*, 0)$, where θ^* is the desired equilibrium for Disk 1 angle. To solve this problem we design a controller using energy shaping and damping injection as described in Section 2. That is, we search for the function V_d and the matrices M_d and J_2 that solve the KE-ME and PE-ME, (8) and (9) respectively. Thus, the energy shaping control is obtained from (10) and the damping injection control from (11).

Since the mass matrix of the DoD is constant and does not depend on the coordinates q, we select M_d as a constant matrix as follows

$$M_d = \begin{bmatrix}\beta_{11} & \beta_{12}\\ \beta_{12} & \beta_{22}\end{bmatrix}$$

where β_{11}, β_{12} and β_{22} are free constants parameters. To simplify the notation, we note

$$M_d M^{-1} = \begin{bmatrix}a & b\\ c & d\end{bmatrix}.$$

Then, the PE-ME (9) results as follows

$$\begin{bmatrix}0 & 1\end{bmatrix}\left\{\begin{bmatrix}0\\ V_0\sin(\varphi)\end{bmatrix} + \begin{bmatrix}a & b\\ c & d\end{bmatrix}\begin{bmatrix}\nabla_\theta V_d\\ \nabla_\varphi V_d\end{bmatrix}\right\} = 0$$
$$V_0\sin(\varphi) + c\,\nabla_\theta V_d + d\,\nabla_\varphi V_d = 0 \tag{14}$$

which a partial differential equation that we should solve for V_d. Using a symbolic software (e.g. Mathematica, Maple), we can verify that a solution of (14)

is

$$V_d(q) = \frac{1}{d}V_0\cos(\varphi) + \frac{k_2}{2}\left(\theta - \frac{c}{d}\varphi - k_1\right)^2 \quad (15)$$

where k_1 and k_2 are free constant parameters.

From the previous selection of M_d, it is clear that the KE-ME (8) is satisfied by choosing the *free parameter* matrix $J_2(q,p) = 0$. In addition, we need to ensure that $M_d > 0$ and that V_d has an isolated minimum at the desired equilibrium $q^\star$. To assign the minimum of V_d, we should ensure that the Jaccobian and Hessian evaluated at $q^\star$ are zero and positive definite respectively. Then, we compute

I) $\nabla_q V_d(q)\big|_{q=q^*} = 0 \Leftrightarrow$

$$\left[\begin{array}{c} k_2\left(\theta - \frac{c}{d}\varphi - k_1\right) \\ \frac{-V_0}{d}\sin(\varphi) - \frac{k_2 c}{d}\left(\theta - \frac{c}{d}\varphi - k_1\right) \end{array}\right]\Bigg|_{q=q^*} = 0$$

which is satisfied if $k_1 = \theta^*$.

II) $\nabla_q^2 V_d(q)\big|_{q=q^*} > 0 \Leftrightarrow$

$$\left[\begin{array}{cc} k_2 & -k_2\frac{c}{d} \\ -k_2\frac{c}{d} & \frac{-V_0}{d}\cos(\varphi) + k_2\left(\frac{c}{d}\right)^2 \end{array}\right]\Bigg|_{q=q^*} > 0$$

which is satisfied provided that $k_2 > 0$ and $d < 0$ (equivalently $\beta_{12}M_{12} - \beta_{22}M_{11} > 0$). In addition, to ensure that $M_d > 0$, the free parameters should satisfy $\beta_{11} > 0$ and $\beta_{11}\beta_{22} - \beta_{12}^2 > 0$. Notice that effectively, the potential energy has a minimum at the desired equilibrium $(\theta^\star, \varphi^\star) = (0,0)$ as shown in Figure 2, where we have used the values of the parameters as in Section 4.1 for illustrative purpose.

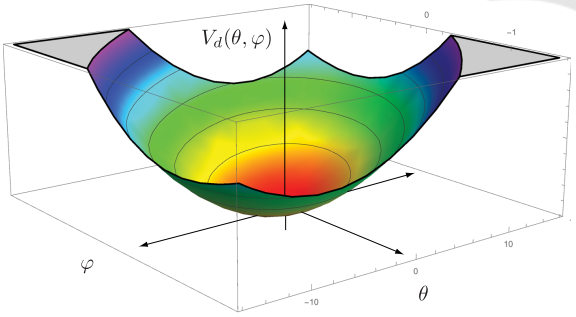

Figure 2: Desired Potential energy.

Finally, the control law is computed from (10) and (11) as follows

$$u = u_{\mathtt{es}} + u_{\mathtt{DI}} = -\frac{b}{d}\nabla_\varphi V - k_2\left(\frac{ad-bc}{d}\right)\times \left(\theta - \frac{c}{d}\varphi - \theta^\star\right) - K_v\, d\,\sigma\left(\dot\theta - \frac{c}{d}\dot\varphi\right) \quad (16)$$

where $\sigma = \frac{M_{11}M_{22} - M_{12}^2}{\beta_{11}\beta_{22} - \beta_{12}^2}$ and the free parameters β_{11}, β_{12}, β_{22}, k_2 and K_v should satisfy

$$\begin{aligned} &\beta_{11} > 0, \quad k_2 > 0, \quad K_v > 0, \\ &\beta_{11}\beta_{22} - \beta_{12}^2 > 0, \\ &\beta_{12}M_{12} - \beta_{22}M_{11} > 0. \end{aligned}$$

Thus, the dynamics of the DoD system (13) in closed loop with the controller (16) can be written in the Hamiltonian form

$$\begin{bmatrix}\dot q \\ \dot p\end{bmatrix} = \begin{bmatrix} 0 & M^{-1}M_d \\ -M_dM^{-1} & -GK_vG^T\end{bmatrix}\begin{bmatrix}\nabla_q H_d \\ \nabla_p H_d\end{bmatrix} \quad (17)$$

To analyse the stability of the closed loop (17), we consider the desired energy H_d in (5) as a Lyapunov candidate function, and we compute its time derivative as follows

$$\begin{aligned} \dot H_d(q,p) &= p^\top M_d^{-1}\dot p + \dot q^\top \dot V_d(q) \\ &= p^\top M_d^{-1}\left(-M_dM^{-1}\dot V_d - GK_vG^\top M_d^{-1}p\right) \\ &\quad + \dot q^\top \dot V_d(q) \\ &= -p^\top M_d^{-1}GK_vG^\top M_d^{-1}p \le 0, \end{aligned}$$

which ensures stability of the desired equilibrium. Asymptotic stability follows from LaSalle's invariance principle (Khalil, 2002), or equivalently from detectability of the signal $y_d = K_vG^\top M_d^{-1}p$ (van der Schaft, 2000).

3.3 Effect of Input Disturbances

Now, we consider the presence of a matched disturbance δ in the closed loop (17). In this case, the closed-loop dynamics is

$$\begin{bmatrix}\dot q \\ \dot p\end{bmatrix} = \begin{bmatrix} 0 & M^{-1}M_d \\ -M_dM^{-1} & -GK_vG^T\end{bmatrix}\begin{bmatrix}\nabla_q H_d \\ \nabla_p H_d\end{bmatrix} + \begin{bmatrix}0 \\ G\end{bmatrix}(v+\delta) \quad (18)$$

where δ is the matched constant disturbance and v is a control input that will be used to reject the unknown disturbance. To obtain the dynamics (18), we use the control $u = u_{\mathtt{es}} + u_{\mathtt{DI}} + v$ in (13), and we add the disturbance. Notice that the disturbance shifts the equilibrium of the closed loop, defined by zero velocities (equivalently $p = 0$), from the desired equilibrium $q^\star$ to a new equilibrium $\bar q$, which is the solution of

$$-M_dM^{-1}\nabla_q V_d + G\delta = 0,$$

which implies that $\bar q = (\bar\theta, \bar\varphi)$ with $\bar\theta = \theta^\star + \frac{d}{(ad-bc)k_2}\delta$ and $\bar\varphi = 0$. This shows that the control objective is not achieved by the controller in the presence of constant disturbances, since θ will not reach the desired value at steady state as desired. This motivates us to implement outer-loop controllers to reject constant unknown disturbances.

3.4 Robust Energy Shaping

In this section, we implement the three integral based controllers proposed by (Donaire et al., 2016) to enhance the robustness of energy shaping controller. We develop these integral controllers for the case of the disk-on-disk in closed loop with the control (16). That is, for the closed-loop dynamics (17) we design a control law v to reject constant disturbances δ. We first present the most complex controller which is a nonlinear PID, and subsequently we present two simpler versions, which result in a type of PI and PID controllers.

3.4.1 Integral Control

The fundamental idea proposed by (Donaire et al., 2016) is to find a dynamic control law $v(q,p,\zeta)$, where ζ is the state of the controller, and a change of coordinates such that the closed loop in the new coordinates can be written as a Hamiltonian system, thus stability is ensured. For the DoD closed loop (18), we proposed a target Hamiltonian system in new coordinates $z \in \mathbb{R}^5$, where we have augmented the state vector by adding the controller state. The target Hamiltonian system is

$$\begin{bmatrix} \dot{z_1} \\ \dot{z_2} \\ \dot{z_3} \end{bmatrix} = \begin{bmatrix} -\Gamma_1 & M^{-1}M_d & -\Gamma_2 \\ -M_dM^{-1} & -GK_vG^T & -GK_3 \\ \Gamma_2^T & K_3^TG^T & -\Gamma_3 \end{bmatrix} \begin{bmatrix} \nabla_{z_1}H_z \\ \nabla_{z_2}H_z \\ \nabla_{z_3}H_z \end{bmatrix} \tag{19}$$

with Hamiltonian

$$H_z(z) = \frac{1}{2}z_2^TM_d^{-1}z_2 + V_d(z_1) + \frac{1}{2}K_I(z_3-\alpha)^2$$

and constant gains equal to

$$\begin{aligned} \Gamma_1 &\triangleq M^{-1}GK_1G^TM^{-1} \\ \Gamma_2 &\triangleq M^{-1}GK_2 \\ \Gamma_3 &\triangleq K_3^TG^TM_d^{-1}GK_2 \\ \alpha &\triangleq \frac{\delta}{K_I\left(K_vG^TM_d^{-1}GK_2+K_3\right)} \end{aligned}$$

where the new coordinates $z = \psi(q,p,\zeta)$ are obtained by the state transformation

$$z_1 = q \tag{20}$$
$$z_2 = p + GK_1G^TM^{-1}\nabla V_d + GK_2K_I(\zeta-\alpha) \tag{21}$$
$$z_3 = \zeta \tag{22}$$

with $K_v>0$, $K_I>0$, $K_1>0$, $K_3>0$ and

$$K_2 = \left(G^TM_d^{-1}G\right)^{-1}.$$

Notice that if we differentiate (20) and replace the derivative of the states by their corresponding state equations from (18) and (19), we obtain the change of coordinates (21), which implies that the state equations of q and z_1 match. The same result is obtained if we differentiate (22) with respect to time, which implies that the state equations of ζ and z_3 also match. Finally, if we differentiate (21) with respect to time, we obtain that the states equations of z_2 and p match if the control law verifies

$$\begin{aligned} v = &-\Big[K_vG^TM_d^{-1}GK_1G^TM^{-1} + K_2K_I \\ &\left(K_2^TG^TM^{-1} + K_3^TG^TM_d^{-1}GK_1G^TM^{-1}\right)\Big]\nabla V_d - \\ &-\left[K_1G^TM^{-1}\nabla^2V_dM^{-1} + K_2K_IK_3^TG^TM_d^{-1}\right]p - \\ &-\left(K_vG^TM_d^{-1}GK_2+K_3\right)K_I\zeta \end{aligned} \tag{23}$$

and

$$\begin{aligned} \dot{\zeta} = &\left(K_2^TG^TM^{-1} + K_3^TG^TM_d^{-1}GK_1G^TM^{-1}\right)\nabla V_d + \\ &+K_3^TG^TM_d^{-1}p. \end{aligned}$$

Since all the state equations of (18) and (19) match, then the dynamics (18) in closed loop with the nonlinear PID controller (23) can be written in the form (19). The Hamiltonian form of the closed-loop dynamics ensures its stability. Indeed, it can be verified straightforward that H_z qualifies as a Lyapunov candidate function for the dynamics (19), and its time derivative is

$$\begin{aligned} \dot{H}_z = &-\nabla^\top V_d(z_1)GM^{-1}K_1G^\top M^{-1}\nabla V_d(z_1) - \\ &z_2^\top M_d^{-1}GK_vG^\top M_d^{-1}z_2 - \Gamma_3K_I^2(z_3-\alpha)^2 \le 0. \end{aligned}$$

Notice that the controller (23) is a nonlinear PID, which we will refer as NLPID2. Moreover, two simpler version of this controller can be obtained by setting the controller parameters to particular values. Indeed, a simpler nonlinear PID can be considering $K_2=0$ and $K_3=1$, which we will refer to as NLPID1, and a nonlinear PI controller is obtained by setting $K_1=0$ and $K_3=0$, which will refer to as NLPI.

In addition, we point out that a controller with only the integral of the passive outputs, which are the velocities form mechanical systems, can be obtained by setting $K_1=0$, $K_2=0$ and $K_3=K_I^{-1}$. We will refer to this controller as IA. It has been shown in (Romero et al., 2013) that this type of integral action does not reject disturbances, destroys the detectability of the passive outputs and creates a manifold of equilibrium. Thus asymptotic stability is not achieved, a fact that is seen in the experiments.

4 EXPERIMENTS

In this section we present experiment results to assess the performance of the controllers presented in Section 3 and verify their applicability in a real setup. The experiments are carried out the prototype show in Figure 3 available at PRISMA Lab. The model parameters of the disk-on-disk are $m_h = 0.52$ Kg, $m_o = 0.22$ Kg, $r_h = 0.15$ m and $r_o = 0.075$ m.

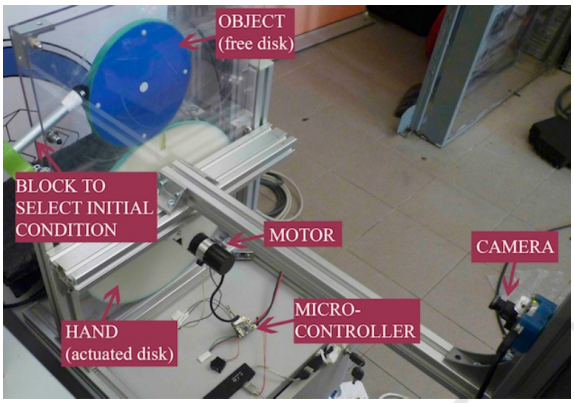

Figure 3: Prototype of the disk-on-disk available at PRISMA Lab.

The prototype consists of two disks placed in between two plastic panels. Disk 1 is actuated by a DC motor (Harmonic Drive RH–8D 3006) equipped with a harmonic drive whose gearhead ratio is 100 : 1, and a 500 p/r quadrature encoder. A rubber band of about 1 mm encircles both disks to avoid slipping. The commands to the motor are provided by an ARM CORTEX M3 microcontroller (32 bit, 75 MHz). This microcontroller receives current references from an external PC through a USB cable. The measurements of Disk 1 are provided by a encoder while the measurements of Disk 2 are provided by an external visual system. This consists of a uEye UI-122-xLE camera providing (376×240) pixel images to the PC at 75 Hz, that is also the controller sample rate. In order to speed up computations, a (15×15) pixel RoI is employed by the image elaboration algorithm running on the same external PC. The control algorithm, which is written in C++, runs on the external PC with a Linux-based operating system.

We have tested five different controllers: i) the standar IDA-PBC controller, ii) the IDA-PBC controller augmented with the IA, iii) the IDA-PBC controller enhanced with the NLPID1, iv) the IDA-PBC controller enhanced with the NLPID2, and v) the IDA-PBC controller enhanced with the NLPI. The experiments are executed under the following scenarios: the initial conditions of the balancing and hand angle positions are $\varphi(0) = 7$ deg and $\theta(0) = 0$ deg respectively, whilst the angular velocities at starting time are zero. The set-point reference for the position of Disk 1 position is set to zero ($\theta^\star = 0$), while Disk 2 has to be stabilized at the upright position. A constant matched disturbance of value $\delta = 0.01$ Nm is added to the system to evaluate the disturbance rejection properties of the controller.

4.1 Standard IDA-PBC

In the first experiment, we evaluate the performance of the IDA-PBC controller (16) stand alone. The parameters of the controller used in the experiment are $\beta_{11} = 0.41$, $\beta_{12} = -0.03$, $\beta_{22} = 0.003$, $k_2 = 0.0005$ and $K_v = 0.08$.

The results of this experiment are shown in Figures 4 to 6. As expected, the controller stabilizes Disk 2 at the upright position as shown in Figure 4. However, it is unable to ensure convergency of the angle of Disk 1 to the desired reference due to the disturbance (see Figure 5). The time history of the control torque is shown in Figure 6, which shows that the controller demands a reasonable torque without large sparks.

4.2 IDA-PBC plus IA

In the second experiment, we test the performance of the IDA-PBC controller plus the IA, that is the controller (16) plus (23) with $K_1 = 0$, $K_2 = 0$ and $K_3 = K_I^{-1}$. The parameters of the controller used in the experiment are $\beta_{11} = 0.41$, $\beta_{12} = -0.03$, $\beta_{22} = 0.003$, $k_2 = 0.0005$, $K_v = 0.08$, and $K_I = 20$.

The results of this experiment are shown in Figures 7-10. Similar to the previous experiment, the controller balances Disk 2 at the upright position, but does not make the angle of Disk 1 converge to zero, which approaches a value of -160 degrees instead (see Figures 7 and 8). The state of the controller is shown in Figure 9, which reaches a value in the equilibrium manifold that has no relation with the disturbance. Finally, the control torque is plotted in Figure 10. This experiment illustrates that the integral action on the velocities does not produce any benefit when used to reject disturbances, as predicted by the theory.

4.3 IDA-PBC plus NLPI

In this fourth experiment, we evaluate the performance of the IDA-PBC controller plus the NLPI, that is the controller (16) plus (23) with $K_1 = 0$ and $K_3 = 0$. The parameters of the controller used in the experiment are $\beta_{11} = 0.41$, $\beta_{12} = -0.03$, $\beta_{22} = 0.003$, $k_2 = 0.0006$, $K_v = 1.5$, $K_2 = \left(G^T M_d^{-1} G\right)^{-1}$ and $K_I = 1.6$.

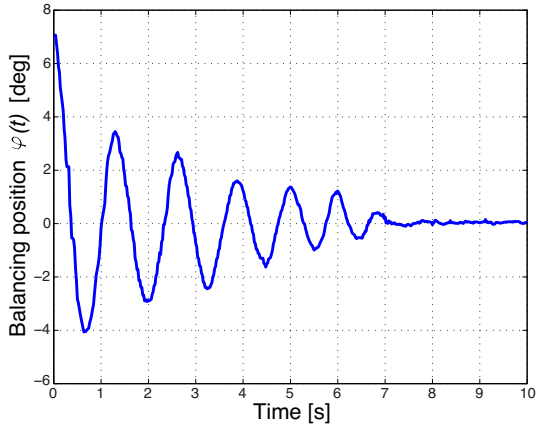

Figure 4: Time history of the balancing angle with the IDA-PBC controller.

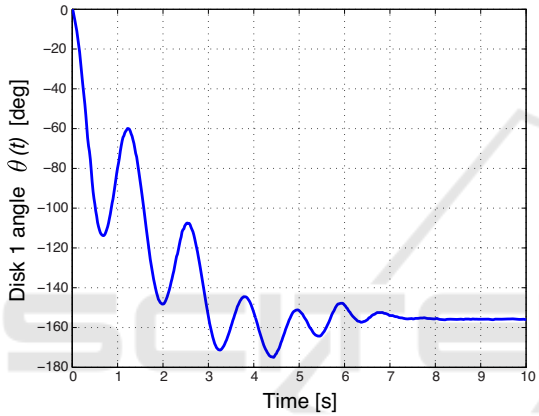

Figure 5: Time history of Disk 1 angle with the IDA-PBC controller.

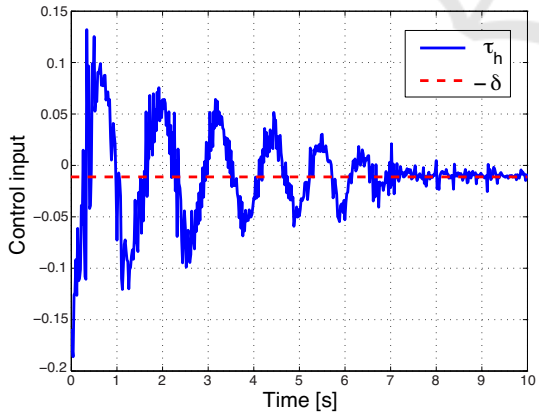

Figure 6: Time history of the control input torque and its value at steady state with the IDA-PBC controller.

The results of this experiment are shown in Figures 11-14. The plots in Figure 11 and 12 show that the controller stabilizes Disk 2 at the upright position and drives Disk 1 to the desired reference angle despite the action of the disturbance. However, a small error (less than one degree) on the angle φ can be seen

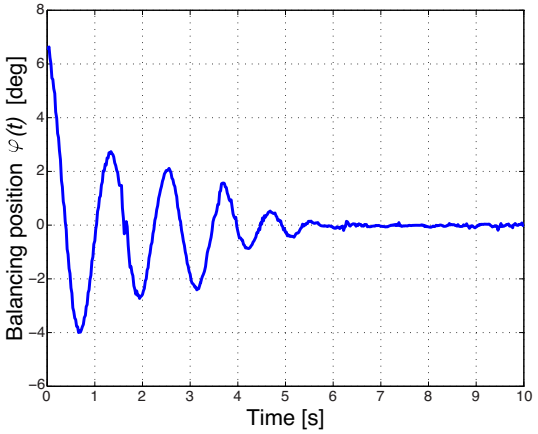

Figure 7: Time history of the balancing angle with the IDA-PBC plus IA controller.

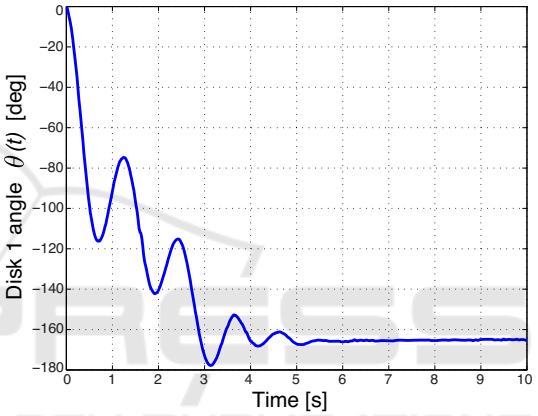

Figure 8: Time history of Disk 1 angle with the IDA-PBC plus IA controller.

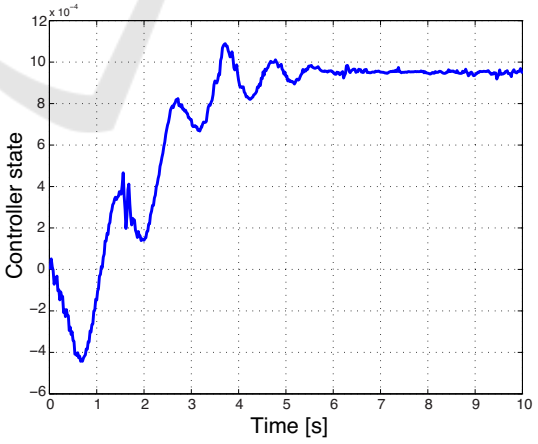

Figure 9: Time history of the controller state and its value at steady state with the IDA-PBC plus IA controller.

in steady state. Figure 13 shows that the state of the controller converges to the value needed to compensate the disturbance, and Figure 14 depicts the control torque, which is bounded between admissible limits.

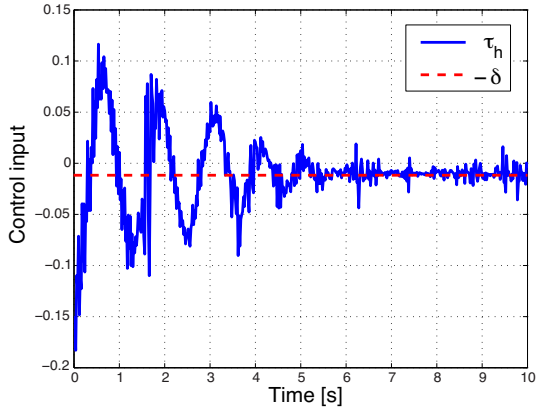

Figure 10: Time history of the control input torque and its value at steady state with the IDA-PBC plus IA controller.

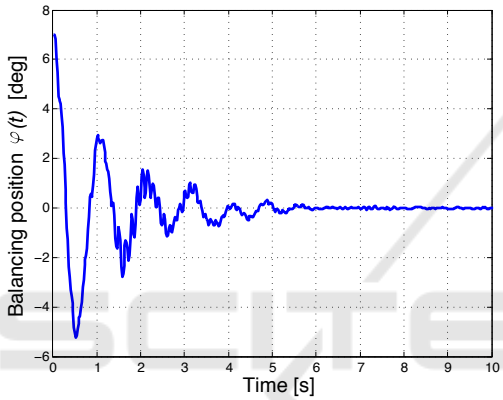

Figure 11: Time history of the balancing angle with the IDA-PBC plus NLPI controller.

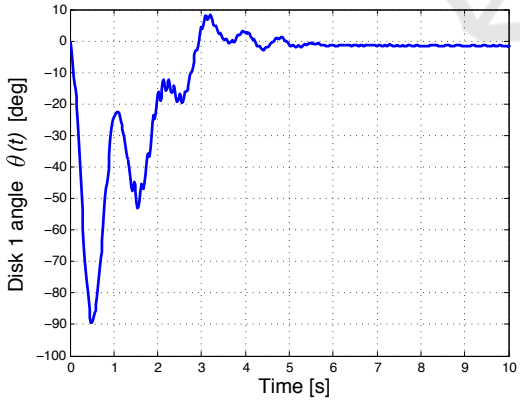

Figure 12: Time history of Disk 1 angle with the IDA-PBC plus NLPI controller.

4.4 IDA-PBC plus NLPID1

In the second set of experiments, we evaluate the performance of the IDA-PBC controller plus the NLPID1, that is the controller (16) plus (23) with $K_2 = 0$ and $K_3 = 1$. The parameters of the controller

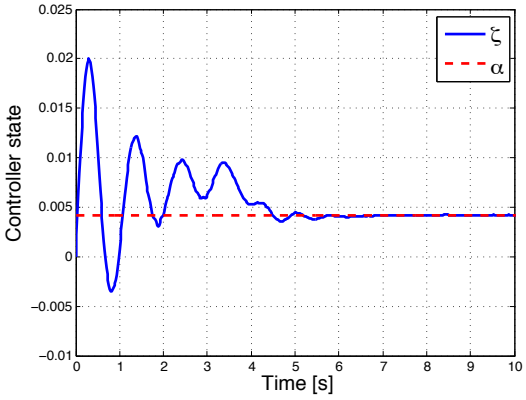

Figure 13: Time history of the controller state and its value at steady state with the IDA-PBC plus NLPI controller.

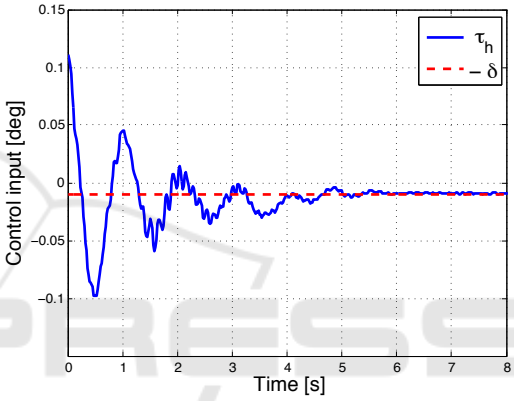

Figure 14: Time history of the control input torque and its value at steady state with the IDA-PBC plus NLPI controller.

are as follows: $\beta_{11} = 0.41$, $\beta_{12} = -0.03$, $\beta_{22} = 0.003$, $k_2 = 0.00048$, $K_1 = 0.00905$, $K_v = 0.35$ and $K_I = 2.3$.

Figures 15 to 18 show the results of this experiment. The time history of the deviation angle of Disk 2 respect to the upright position is depicted in Figure 15. This figure shows that Disk 2 is balanced as desired. Figure 16 shows that the angle of Disk 1 reaches the reference value, and the controller rejects the disturbance. Also, it can be seen in Figure 17 that the controller state produces an estimate of the disturbance, which is used to compensate it. In addition, the control input is shown in Figure 18.

4.5 IDA-PBC plus NLPID2

In the last experiment, we evaluate the performance of the IDA-PBC controller plus the NLPID2, that is the controller (16) plus (23). The parameters of the controller are as follows: $\beta_{11} = 0.41$, $\beta_{12} = -0.03$, $\beta_{22} = 0.003$, $k_2 = 0.00025$, $K_1 = 0.012$, $K_2 = \left(G^T M_d^{-1} G\right)^{-1}$, $K_3 = 0.06$, $K_v = 0.3$ and $K_I = 2.2$.

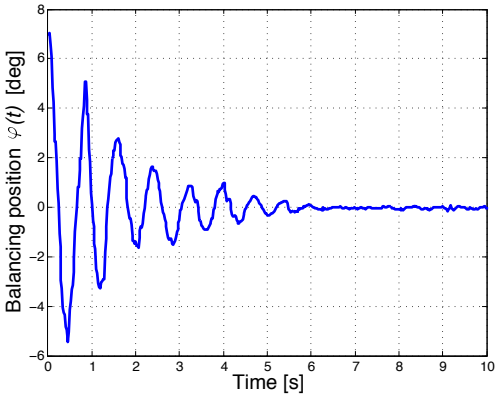

Figure 15: Time history of the balancing angle with the IDA-PBC plus NLPID1 controller.

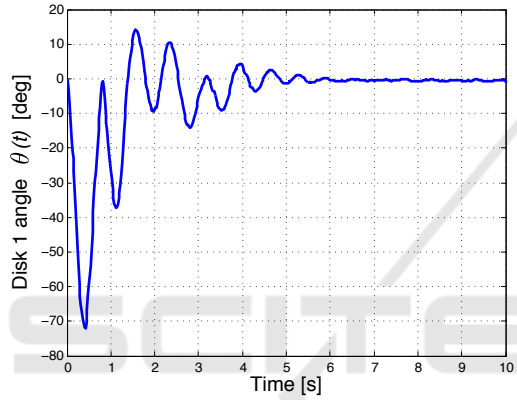

Figure 16: Time history of Disk 1 angle with the IDA-PBC plus NLPID1 controller.

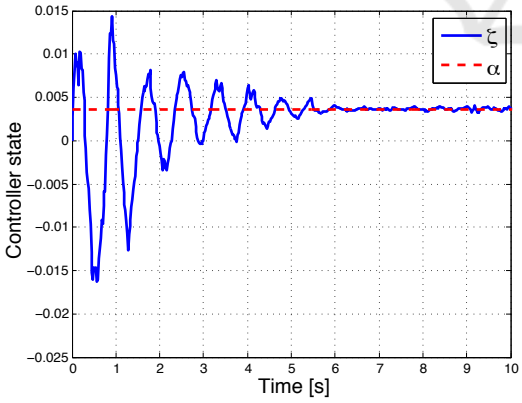

Figure 17: Time history of the controller state and its value at steady state with the IDA-PBC plus NLPID1 controller.

The time history of the most significant variables obtained in this experiment are shown in Figures 19 to 22. As can be seen in Figures 19 and 20, the controller is able to balance Disk 2 at the upright position while stabilizing the angle of Disk 1 at the desired set-point. The controller state and the control torque are

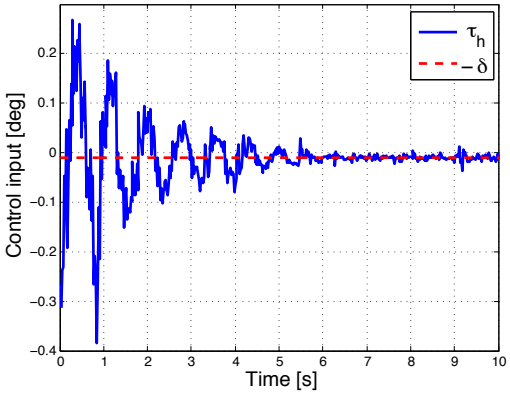

Figure 18: Time history of the control input torque and its value at steady state with the IDA-PBC plus NLPID1 controller.

shown in Figures 21 and 22, respectively. These plots evidence that the controller ensures internal stability, output regulation and disturbance rejection showing very good performance.

4.6 Discussion

First, we notice that although IDA-PBC controllers show robustness against parameter uncertainties, the action of disturbance can greatly deteriorate the performance of the closed loop, as shown in the experiments. Indeed, the IDA-PBC controller balances Disk 2, but the steady-state error of Disk 1 angle is notably large. The addition of integral action on the passive output, which is the most intuitive solutions, does not improve the performance of the controller respect to the standard IDA-PBC. This fact has been proved in (Romero et al., 2013), however no experiment has illustrated this theoretical results before.

The last three controllers tested are able to balance Disk 2 and simultaneously stabilize the angle of Disk 1, thanks to the action of the outer NLPID. However, from the plots we can see that the convergency of the variables of the disk-on-disk using the controller NLPI is faster that the NLPID1, and produces less oscillations. This better transient performance is, however, darken by the steady state error, which is not present in the NLPID1. Also, the overshoot of Disk 1 angle is greater when using NLPI compared with the NLPID1 at expense of a more demanding control torque. On the other side, the last experiment shows that the controller NLPID2 performs better than the controller NLPI and NLPID1. Indeed, the transient performance of the NLPID2 is better that the other controllers with less overshoot in both the balancing angle φ related to Disk 2 and the angle θ of Disk 1. These angles reach their desired values with less os-

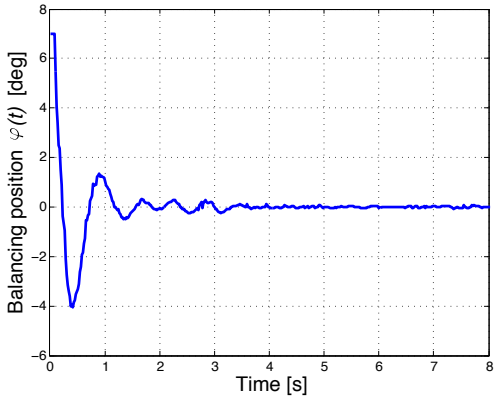

Figure 19: Time history of the balancing angle with the IDA-PBC plus NLPID2 controller.

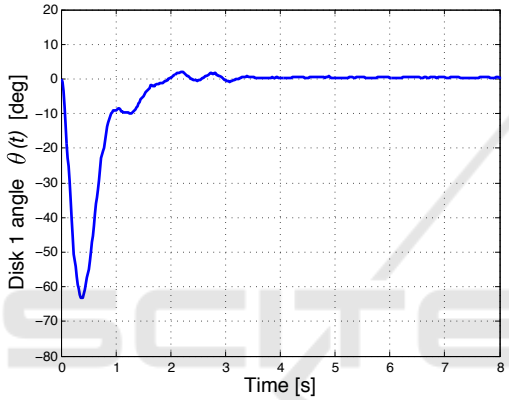

Figure 20: Time history of Disk 1 angle with the IDA-PBC plus NLPID2 controller.

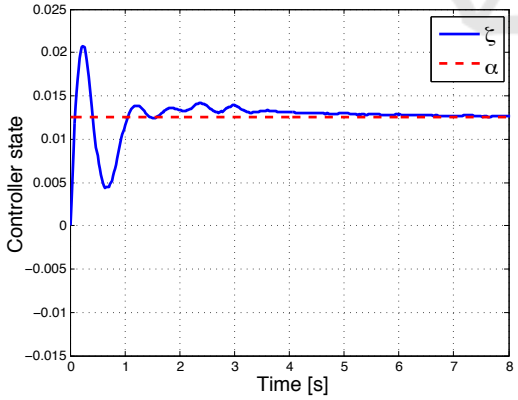

Figure 21: Time history of the controller state and its value at steady state with the IDA-PBC plus NLPID2 controller.

cillations and with a faster rate of convergency. In addition, the control torque demanded by the controller NLPID2 looks less demanding and smoother than that of the controllers NLPI and NLPID1. As one may expect, all these benefits are at expenses of a more complex controller.

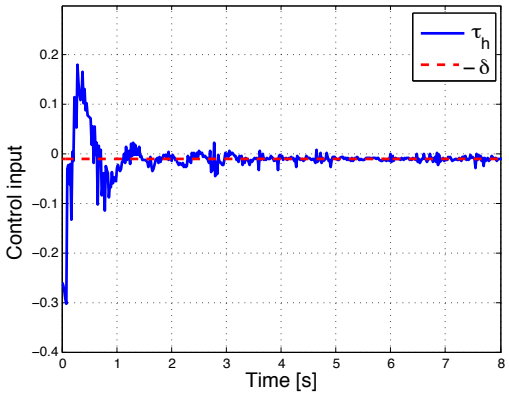

Figure 22: Time history of the control input torque and its value at steady state with the IDA-PBC plus NLPID2 controller.

The DoD setup could be also stabilized in principle by a linear controller, for example using a LQR controller plus integral action for disturbance rejection. However, the control design is based on a linear approximation, which is only valid on a small neighbourhood of the equilibrium. The advantage of nonlinear controllers is that the basin of attraction of the closed loop can be theoretically probe to be larger than a small vicinity around the equilibrium.

A video that summarises the experiments of the DoD system described in Sections 4.3, 4.4 and 4.5 can be watched on https://youtu.be/B0k8JtYZjrY.

5 CONCLUSION

In this paper we present three robust IDA-PBC controllers for the disk-on-disk system subject to matched disturbances. We also show experimental results to evaluate the related performance and asses the applicability of advanced nonlinear control techniques based on passivity in a real setup. The results evidence that the robust IDA-PBC has good performance and validate the use of this technique on a practical application. Motivated by this positive result, in future work we intend to design controllers for more complex mechanical system performing more difficult tasks.

ACKNOWLEDGEMENTS

This work was partially supported by the RoDyMan project, which has received funding from the European Research Council FP7 Ideas under Advanced Grant agreement number 320992. The authors are solely responsible for the content of this manuscript.

The first author acknowledges the National University of Rosario for supporting his internship at PRISMA Lab.

REFERENCES

Donaire, A. and Junco, S. (2009). On the addition of integral action to port-controlled Hamiltonian systems. *Automatica*, 45:1910–1916.

Donaire, A., Romero, J. G., Ortega, R., and Siciliano, B. (2016). Robust IDA-PBC for underactuated mechanical systems subject to matched disturbances. In *American Control Conference*, Boston, USA.

Haddad, W. and Chellaboina, V. (2007). *Nonlinear Dynamical Systems and Control. A Lyapunov-Based Approach*. Princeton University Press, New Jersey.

Khalil, H. (2002). *Nonlinear Systems*. Prentice Hall.

Lanczos, C. (1960). The variational principles of mechanics. *University of Toronto Press*.

Lippiello, V., Ruggiero, F., and Siciliano, B. (2016). The effect of shapes in input-state linearization for stabilization of nonprehensile planar rolling dynamic manipulation. *IEEE Robotics and Automation Letters*, 1(1):492–499.

Merkin, D. (1997). *Introduction to the Theory of Stability*. Springer Verlag, New York.

Ortega, R., Donaire, A., and Romero, J. G. (2016). *Passivity–based control of mechanical systems*. Lecture Notes in Control and Information Sciences. Springer, Berlin/Heidelberg.

Ortega, R., Loría, A., Nicklasson, P., and Sira-Ramírez, H. (1998). *Passivity-based Control of Euler-Lagrange Systems: Mechanical, Electrical, and Electromechanical Applications*. Springer Verlag, London.

Ortega, R. and Romero, J. G. (2012). Robust integral control of port-Hamiltonian systems: The case of non-passive outputs with unmatched disturbances. *Systems & Control Letters*, 61(1):11–17.

Ortega, R., Spong, M., Gomez-Estern, F., and Blankenstein, G. (2002). Stabilization of a class of underactuated mechanical systems via interconnection and damping assignment. *IEEE Transactions on Automatic Control*, 47(8):1218–1233.

Romero, J. G., Donaire, A., and Ortega, R. (2013). Robust energy shaping contorl of mechanical systems. *Systems & Control Letters*, 62(9):770–780.

Ryu, J. C., Ruggiero, F., and Lynch, K. (2013). Control of nonprehensile rolling manipulation: Balancing a disk on a disk. *IEEE Transactions on Robotics*, 29(5):1152–1161.

Ryu, J. C., Ruggiero, F., and Lynch, K. M. (2012). Control of nonprehensile rolling manipulation: Balancing a disk on a disk. In *IEEE International Conference on Robotics and Automation*, pages 3232–3237, St. Paul, USA.

Siciliano, B., Sciavicco, L., Villani, L., and Oriolo, G. (2009). *Robotics. Modelling, Planning and Control*. Springer Verlag, London.

Spong, M., Hutchinson, S., and Vidyasagar, M. (2006). *Robot Modeling and Control*. John Wiley & Sons, USA.

van der Schaft, A. J. (2000). *L2-gain and Passivity Techniques in Nonlinear Control*. Springer Verlag.